Journal of Advanced Ceramics
2018, **7**(3): 237–245
https://doi.org/10.1007/s40145-018-0275-3
ISSN 2226-4108
CN 10-1154/TQ

Research Article

Carbon dioxide adsorption of two-dimensional carbide MXenes

Bingxin WANG[a,b], Aiguo ZHOU[a,b,*], Fanfan LIU[a,b], Jianliang CAO[c], Libo WANG[a,b], Qianku HU[a,b]

[a]*School of Materials Science and Engineering, Henan Polytechnic University, Jiaozuo 454000, China*
[b]*Henan International Joint Research Laboratory for High-Performance Light Metallic Materials and Numerical Simulations, Henan Polytechnic University, Jiaozuo 454000, China*
[c]*School of Chemistry and Chemical Engineering, Henan Polytechnic University, Jiaozuo 454000, China*

Received: September 28, 2017; Revised: March 30, 2018; Accepted: April 02, 2018

Abstract: Two-dimensional carbide MXenes ($Ti_3C_2T_x$ and V_2CT_x) were prepared by exfoliating MAX phases (Ti_3AlC_2 and V_2AlC) powders in the solution of sodium fluoride (NaF) and hydrochloric acid (HCl). The specific surface area (SSA) of as-prepared $Ti_3C_2T_x$ was 21 m^2/g, and that of V_2CT_x was 9 m^2/g. After intercalation with dimethylsulfoxide, the SSA of $Ti_3C_2T_x$ was increased to 66 m^2/g; that of V_2CT_x was increased to 19 m^2/g. Their adsorption properties on carbon dioxide (CO_2) were investigated under 0–4 MPa at room temperature (298 K). Intercalated $Ti_3C_2T_x$ had the adsorption capacity of 5.79 mmol/g, which is close to the capacity of many common sorbents. The theoretical capacity of $Ti_3C_2T_x$ with the SSA of 496 m^2/g was up to 44.2 mmol/g. Additionally, due to high pack density, MXenes had very high volume-uptake capacity. The capacity of intercalated $Ti_3C_2T_x$ measured in this paper was 502 $V \cdot v^{-1}$. This value is already higher than volume capacity of most known sorbents. These results suggest that MXenes have some advantage features to be researched as novel CO_2 capture materials.

Keywords: MXenes; specific surface area (SSA); adsorption; carbon dioxide

1 Introduction

Carbon dioxide (CO_2) is the most relevant contributor to greenhouse effect. However, over the past decades, the emission of CO_2 and other greenhouse gases is continuously increased. Anthropogenic CO_2 emissions are mainly due to combustion process, and a number of other industrial processes, such as hydrogen production, give some contributions also. In order to decrease CO_2 content in atmosphere, it is necessary to look for a suitable material to adsorb and capture CO_2.

In general, pressure and/or temperature swing approaches are used to capture CO_2 in porous materials. The porous materials, as CO_2 sorbents, should have superior properties in terms of capacity, stability, kinetics, selectivity, and regeneration [1]. Up to now, a wide range of sorbents for CO_2 capture, have been used and studied, including metal organic frameworks (MOFs) [2], functionalized porous silica [3], activated carbon [4], zeolites [5], metal oxides, and microporous polymers [6]. Among these sorbents, MOFs exhibit very high CO_2 uptake up to 54.4 mmol/g under high pressures (5 MPa) at 298 K [2]. Despite the excellent adsorption capacities, MOFs are much more expensive

* Corresponding author.
E-mail: zhouag@hpu.edu.cn

than commercially available activated carbons. In addition, MOFs are water sensitive; they can chemisorb water, and/or their porous structure can be destroyed upon exposure to water vapor. Up to now, it is still a great deal of research effort to design and synthesize high performance porous materials for CO_2 sorbents.

In 2011, a two-dimensional (2D) transition metal carbide with the name of MXene was prepared [7] and gained significant attention due to their excellent properties in many fields [8–12]. MXenes are prepared by selectively etching away A-site element from MAX ($M_{n+1}AX_n$) phases with hydrofluoric acid or fluoride salt solution [7,13], where M is an early transition metal, A usually belongs to the groups IIIA and IVA, and X is carbon and/or nitrogen. Due to high surface energy, the surface of MXenes prepared in etching solution is always terminated with F, OH, and/or O [14]. Thus $M_{n+1}X_nT_x$ is normally used as the chemical formula of MXene, where T_x represents the terminated F, OH, or O groups. By now, more than 10 MXenes, $Ti_3C_2T_x$ [15], Ti_2CT_x [16], V_2CT_x [17], etc, have been successfully synthesized and many more are predicted [18–22].

Due to the unique structure and properties, MXenes are extensively researched in many areas, such as microwave absorption and shielding [23–25], supercapacitors [26,27], ion battery [21,28–30], etc. Moreover, due to stacking structure, MXenes have a large amount of interlayer space. The interlayer space is suitable for gas adsorption. From theoretical calculation [31], MXenes with oxygen functional groups could adsorb NH_3, H_2, CO, CO_2, etc. Our group has investigated the adsorption properties of MXene on some gases through theories and experiments, and found that MXenes can have important application in hydrogen storage [8,32] and methane adsorption [16,33]. At present, as the authors know, there is no research on the CO_2 adsorption of MXenes.

Following this idea, in this work, we synthesized two kinds of MXenes: $Ti_3C_2T_x$, V_2CT_x, and researched the CO_2 adsorption of MXenes. The main purpose of this work was to clarify the relation between MXenes' microstructure and their CO_2 adsorption properties. And based on this work, the possibility of employing them as carbon dioxide capture media was explored.

2 Experiments

2. 1 MXene nanosheets preparation

MXenes ($Ti_3C_2T_x$, V_2CT_x) with 2D structure in this work were produced by immersing MAX phase (Ti_3AlC_2, V_2AlC) powders in etching solution. Ti_3AlC_2 powders and V_2AlC powders were synthesized in a tube furnace. The experimental details to synthesize those powders were reported in Ref. [34] for Ti_3AlC_2 powders and in Refs. [35,36] for V_2AlC powders. The etching solution was composed of NaF (≥ 99.8 wt%, Sinopharm Chemical Reagent Co., Beijing, China) and HCl (6 mol/L, Shuangshuang Chemical Co., Yantai, China) solution. 2 g Ti_3AlC_2 powders were soaked in NaF (2 g) and HCl (40 mL) solution at 333 K for 48 h to obtain $Ti_3C_2T_x$. 2 g V_2AlC powders were soaked in NaF (2 g) and HCl (40 mL) solution at 363 K for 72 h to obtain V_2CT_x. After etching, powders were separated from the solution by centrifugation, washed with deionized water and ethanol repeatedly. The obtained MXene powders were dried in vacuum at 353 K. Thereafter, MXene powders were collected for testing and were labeled as as-$Ti_3C_2T_x$ or as-V_2CT_x in this paper.

As-prepared MXenes were further exfoliated by intercalation with dimethylsulfoxide (DMSO). 0.5 g MXene ($Ti_3C_2T_x$ or V_2CT_x) powders were mixed with 10 mL DMSO and then magnetically stirred for 18 h at room temperature [37]. Thereafter, the samples were washed several times by deionized water and then dried in a vacuum oven at 353 K. The MXene after intercalation was labeled as int-$Ti_3C_2T_x$ or int-V_2CT_x in this paper.

2. 2 Characterization

X-ray diffraction (XRD) patterns of MAX (Ti_3AlC_2, V_2AlC) and MXene ($Ti_3C_2T_x$, V_2CT_x) powders were obtained with an X-ray diffractometer (Rigaku, Samart-lab, Japan) with Cu Kα radiation (λ = 1.5406 Å). All XRD samples were prepared by tiling powders on a flat sample holder. The morphology and microstructures of samples were observed by a field emission scanning electron microscopy (FE-SEM, Merlin Compact, Carl Zeiss NTS GmbH, Germany) and a transmission electron microscope (TEM, JEOLJEM-2010, Japan) with an accelerating voltage of 200 kV. TEM samples were prepared by ultrasonically dispersing MXene powders in ethylalcohol and then moving them to a copper grid. Raman spectrum was recorded with a confocal spectrometer (Horiba JobinYvon, LabRAM HR800, French), using the 514.5 nm excitation of the argon laser at room temperature. X-ray photoelectron spectroscopy (XPS) analyses were performed with a Surface Sciences Instruments spectrometer (PHI X-tool, Ulvac-Phi,

Japan) using a focused monochromatized Al Kα radiation (1486.6 eV).

2. 3 Adsorption test

Prior to all adsorption measurements, the samples were degassed in vacuum at 353 K for 2 h.

Nitrogen adsorption isotherms of MXenes were measured at 77 K (Quantachrome, Autosorb-iO-MP, USA). The obtained nitrogen adsorption–desorption isotherms were evaluated to give the pore parameters, including specific surface area, pore-size distribution, and total pore volume.

Adsorption of CO_2 was measured by high temperature and high pressure gas adsorption instrument (Gold APP, H-Sorb 2600, Beijing, China). Before adsorption, 0.4 g MXene powers were placed in a cylindrical container. Carbon dioxide isotherms of $Ti_3C_2T_x$ and V_2CT_x were obtained at 298 K under 0–4 MPa.

3 Results and discussion

3. 1 Characterization of samples

The X-ray diffraction (XRD) patterns of MAX phases, as-prepared MXenes, and intercalated MXenes are shown in Fig. 1. The values of lattice parameter *c* calculated from XRD patterns are listed in Table 1. Because cation and water molecules can enter the interlayer space, hydrate the intercalated cation, and expand the layers [38], *c* of MXene is changeable with process conditions. Larger *c* means larger interlayer space. The intensity ratios of MAX's (002) peak to MXene's (002) peak, I_{MAX}/I_{MXene}, are also listed in Table 1, which represent the amount of residual MAX phase in the obtained MXene.

(1) $Ti_3C_2T_x$. From the XRD pattern of Fig. 1(a), it is evident that the (002) peak of Ti_3AlC_2, which is initially at $2\theta \approx 9.5°$, is broadened and shifted to lower angle (7.53°) after exfoliation by NaF and HCl for 48 h at 333 K. The new peak belongs to $Ti_3C_2T_x$ MXene. The lattice parameter *c* of Ti_3AlC_2 is calculated to be 18.6 Å and *c* of as-$Ti_3C_2T_x$ is 23.4 Å. After intercalation, the $Ti_3C_2T_x$ was further exfoliated and *c* of intercalated $Ti_3C_2T_x$ (int-$Ti_3C_2T_x$) is 27.6 Å. I_{MAX}/I_{MXene} of as-$Ti_3C_2T_x$ is ~0.036. This means there is residual Ti_3AlC_2 in the $Ti_3C_2T_x$. However, the purity is enough for property characterization. After DMSO intercalation, the (002) peak of int-$Ti_3C_2T_x$ is shifted to low angle (6.41°) and *c* is increased from 23.4 to 27.6 Å. I_{MAX}/I_{MXene} of int-$Ti_3C_2T_x$ is ~0.037, similar with the value of as-$Ti_3C_2T_x$, which indicates that the purity of $Ti_3C_2T_x$ is almost unchangeable during the intercalation. Therefore, the intercalation can further exfoliate $Ti_3C_2T_x$ MXene and it is an effective way to obtain $Ti_3C_2T_x$ with larger interlayer space.

(2) V_2CT_x. In Fig. 1(b), (002) peak of V_2AlC at 13.5° almost disappears after etching and a new peak at ~8.05° appears, which belongs to V_2CT_x MXene. I_{MAX}/I_{MXene} (Table 1) of as-V_2CT_x is ~0.092. This value is similar with the previous reported value in literature [17]. And V_2CT_x made by NaF+HCl etching is much purer than V_2CT_x made by HF etching, which has

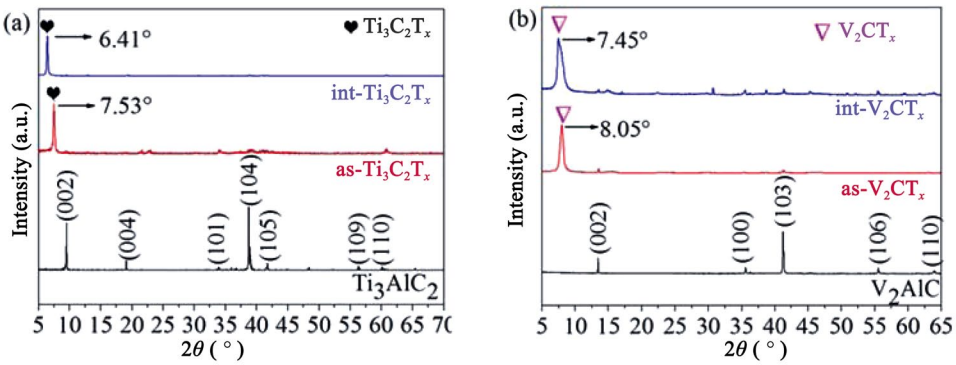

Fig. 1 XRD patterns of MAX phases, as-MXenes, and int-MXenes: (a) Ti_3AlC_2 and $Ti_3C_2T_x$, (b) V_2AlC and V_2CT_x.

Table 1 XRD data of MAX phases and MXenes. Lattice parameter *c* was calculated from 2θ of (002) peak and I_{MAX}/I_{MXene} is intensity ratio of MAX's (002) peak to MXene's (002) peak

	Ti_3AlC_2	as-$Ti_3C_2T_x$	int-$Ti_3C_2T_x$	V_2AlC	as-V_2CT_x	int-V_2CT_x
Lattice parameter *c* (Å)	18.6	23.4	27.6	13.1	21.9	23.7
I_{MAX}/I_{MXene}	—	0.036	0.037	—	0.092	0.093

I_{MAX}/I_{MXene} of ~1.06 [39]. I_{MAX}/I_{MXene} of int-V_2CT_x is ~0.093, similar with the value of as-V_2CT_x, which also indicates that the purity of V_2CT_x is almost unchangeable during the intercalation. As shown in Table 1, c of V_2AlC is 13.1 Å. After exfoliation, c of as-V_2CT_x is 21.9 Å. After intercalation, c of int-V_2CT_x increases to 23.7 Å. Similar with $Ti_3C_2T_x$, after intercalation with DMSO, V_2CT_x is further exfoliated and space between MXene layers becomes larger.

The SEM image of as-$Ti_3C_2T_x$ is shown in Fig. 2(a); the inset is the SEM image of int-$Ti_3C_2T_x$. The SEM image of as-V_2CT_x is shown in Fig. 2(b); that of int-V_2CT_x is shown in the inset of Fig. 2(b). The MXene samples in this paper have typical multi-layer stack morphology of MXene [7].

The TEM image of fully exfoliated $Ti_3C_2T_x$ flakes is shown in Fig. 3(a) and that of V_2CT_x is shown in Fig. 3(b). From Fig. 3, the MXene sheets are quite thin and transparent to electrons [7,17]. The edge of the flake has significant curl, indicating that the V_2CT_x layer is very thin and has certain toughness.

Figure 4 is the Raman spectra of $Ti_3C_2T_x$ and V_2CT_x. For $Ti_3C_2T_x$, the Raman spectrum is similar with previous report spectrum in literature [40]. The bands assigned to Al–Ti vibrations of precursor Ti_3AlC_2 at 185 and 272 cm^{-1} are vanished. The bands at 154, 204, and 623 cm^{-1} involve Ti–C vibrations [41]. From the Raman spectrum, $Ti_3C_2T_x$ is successfully synthesized.

For V_2CT_x, the bands of V_2AlC at 157, 239, 257, and 364 cm^{-1} [41] are vanished and new bands appear at 139, 254, 490, and 667 cm^{-1}. This spectrum is similar with the reported spectrum of V_2C MXene in a very recent literature [42]. Thus, V_2CT_x is successfully synthesized.

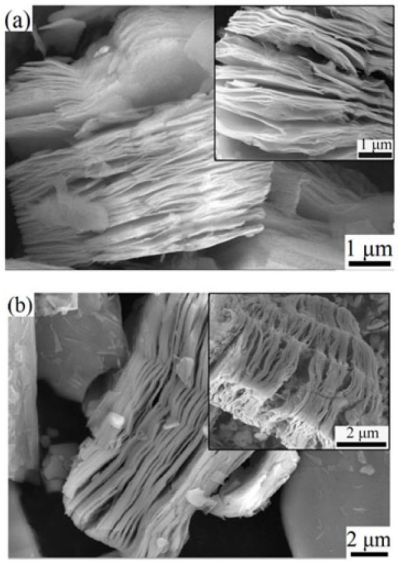

Fig. 2 SEM images of (a) $Ti_3C_2T_x$ and (b) V_2CT_x. The insets are int-$Ti_3C_2T_x$ and int-V_2CT_x, respectively.

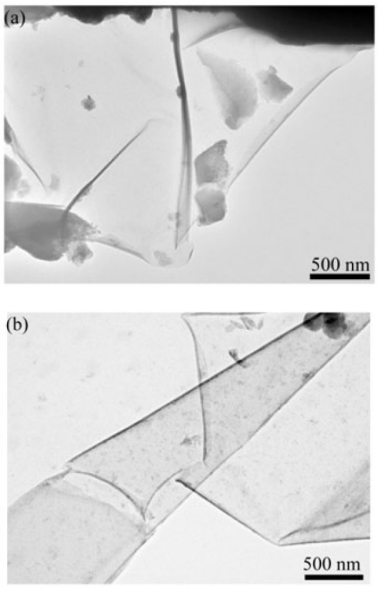

Fig. 3 TEM images of (a) $Ti_3C_2T_x$ and (b) V_2CT_x.

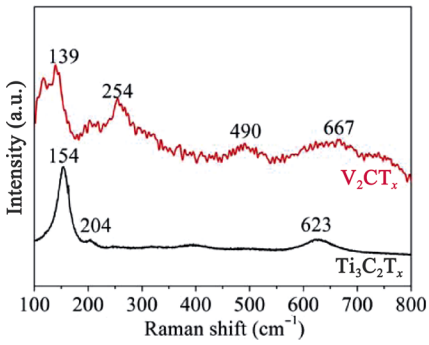

Fig. 4 Raman spectra of $Ti_3C_2T_x$ and V_2CT_x.

3. 2 Surface area and porosity analysis of MXenes

The N_2 adsorption–desorption isotherms at 77 K and pore size distribution of as-MXenes and int-MXenes are shown in Fig. 5. According to IUPAC (International Union of Pure and Applied Chemistry) classification, all N_2 adsorption–desorption isotherms of MXenes are of type IV and exhibit a hysteresis loop, showing the existence of mesopores in MXenes. The corresponding pore size distributions of MXenes are calculated by BJH model and are shown in the insets of Fig. 5.

In Fig. 5(a), for as-$Ti_3C_2T_x$, its SSA is calculated to be 21 m^2/g. The total pore volume of this $Ti_3C_2T_x$ sample is obtained to be 0.08 cm^3/g at the relative pressure P/P_0 = 0.99. In Fig. 5(b), after intercalation, the SSA of int-$Ti_3C_2T_x$ is 66 m^2/g and the total pore

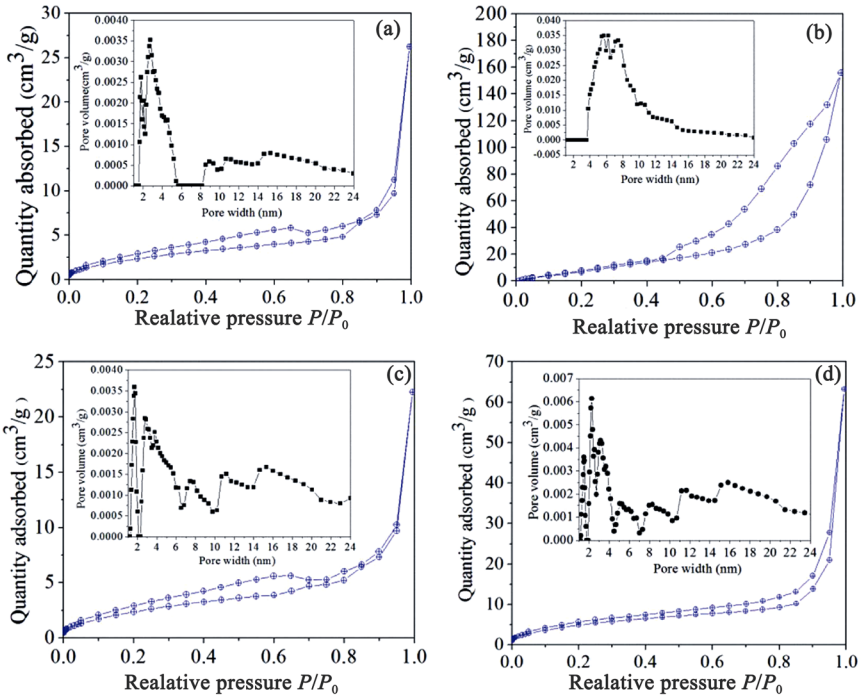

Fig. 5 N_2 sorption isotherms and pore size distributions of MXenes: (a) as-$Ti_3C_2T_x$, (b) int-$Ti_3C_2T_x$, (c) as-V_2CT_x, (d) int-V_2CT_x.

volume is 0.25 cm^3/g. The pore width of as-$Ti_3C_2T_x$ is distributed in the range of 1.8–24 nm. After intercalation, the pore width of int-$Ti_3C_2T_x$ is distributed in the range of 3.9–24 nm. Additionally, the pore volume of int-$Ti_3C_2T_x$ is much larger than that of as-$Ti_3C_2T_x$. Thus, it can be concluded that the intercalation process really increases the distance between $Ti_3C_2T_x$ layers, which, in turn, enlarges the interlayer space for gas adsorption.

In Fig. 5(c), for as-V_2CT_x, the SSA is 9 m^2/g and total pore volume is 0.04 cm^3/g, both smaller than $Ti_3C_2T_x$. It is because that the exfoliation of V_2CT_x is not as good as $Ti_3C_2T_x$ and there is not enough interlayer space in V_2CT_x MXene. In Fig. 5(d), after intercalation, the SSA of V_2CT_x is 19 m^2/g and total pore volume is 0.09 cm^3/g. The intercalation can increase the SSA and pore volume of V_2CT_x; however, the effect is less obvious than that for $Ti_3C_2T_x$.

3. 3 CO_2 adsorptive property of MXenes

CO_2 adsorption and desorption isotherms of as-MXenes and int-MXenes are shown in Fig. 6. According to theoretical calculation [31], only monolayer CO_2 molecules can be adsorbed on the surface of MXenes with O termination. Thus, Langmuir isotherm assumption is used to analyze the CO_2 adsorption of MXenes.

Figure 6(a) shows CO_2 adsorption and desorption curves of as-$Ti_3C_2T_x$ and int-$Ti_3C_2T_x$ under 0–4 MPa at 298 K. For as-$Ti_3C_2T_x$, the CO_2 adsorbed amount is 1.33 mmol/g at 4 MPa; after intercalation with DMSO, the adsorbed amount is 5.79 mmol/g. The new value is 4.3 times of the previous adsorbed amount. It is obvious that intercalation can dramatically increase the adsorbed amount of $Ti_3C_2T_x$. As discussed in Section

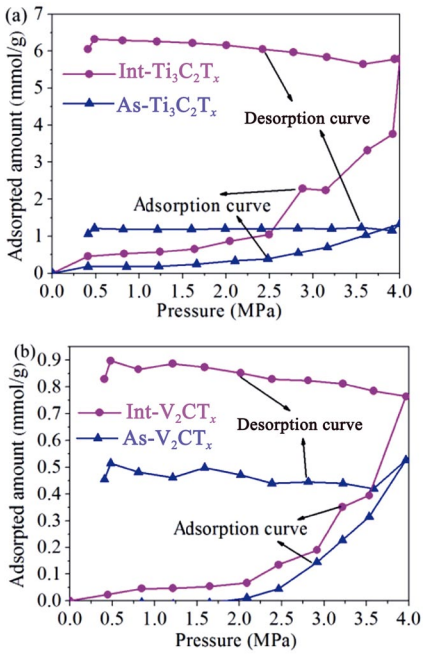

Fig. 6 CO_2 adsorption and desorption curves of MXenes at 298 K under 0–4 MPa: (a) as-$Ti_3C_2T_x$ and int-$Ti_3C_2T_x$, (b) as-V_2CT_x and int-V_2CT_x.

3.2, compared with as-$Ti_3C_2T_x$, int-$Ti_3C_2T_x$ has larger SSA, higher pore volume, and most pores have larger pore width. These factors are favorable for MXenes to adsorb CO_2.

Figure 6(b) represents the CO_2 adsorption and desorption curves of as-V_2CT_x and int-V_2CT_x under 0–4 MPa at 298 K. Unlike $Ti_3C_2T_x$, V_2CT_x has no adsorption capacity of CO_2 if the pressure is less than ~2 MPa. It is because V_2CT_x has smaller interlayer space for gas adsorption or the space is blocked by intercalation molecules, and some pressure is required to squeeze CO_2 into the pores. With the pressure increasing, CO_2 molecules begin to come into the interlayer space of V_2CT_x and the CO_2 adsorbed amount is 0.52 mmol/g at 4 MPa as shown in Fig. 6(b). After intercalation with DMSO, the CO_2 adsorbed amount is 0.77 mmol/g at 4 MPa.

From the results in Fig. 6, it can be concluded that the MXenes, no matter $Ti_3C_2T_x$ or V_2CT_x, no matter as-prepared or intercalated, can adsorb CO_2. From the desorption curves in Fig. 6, the adsorbed CO_2 cannot be released under atmospheric pressure. Therefore, MXenes can be used as sorbent to capture CO_2. From the shape of adsorption curves in Fig. 6, the mesoporous in MXenes to adsorb CO_2 are slit-like. This agrees well with the morphology of MXene. The interlayer space in slit-like shape is the room to adsorb and storage gas molecules. This is obviously different with porous carbon, which has type I adsorption curve, corresponding to narrow micropores (< 1 nm) as shown in Ref. [43].

In order to verify whether there are microstructure and composition change of MXene after the adsorption, XRD patterns and SEM images of int-MXenes after CO_2 adsorption were obtained and are shown in Figs. 7(a) and 7(b). From the XRD patterns, after the adsorption, the (002) peaks of int-MXenes shift to small angle direction. This indicates that CO_2 enters the MXene layers and increases the distance between layers. In addition, there are no diffraction peaks of other substances. And from the SEM images, int-MXenes after CO_2 adsorption still maintain the two-dimensional layered structure without detectible change. These results indicate that adsorption of CO_2 by MXene has the characters of physical adsorption.

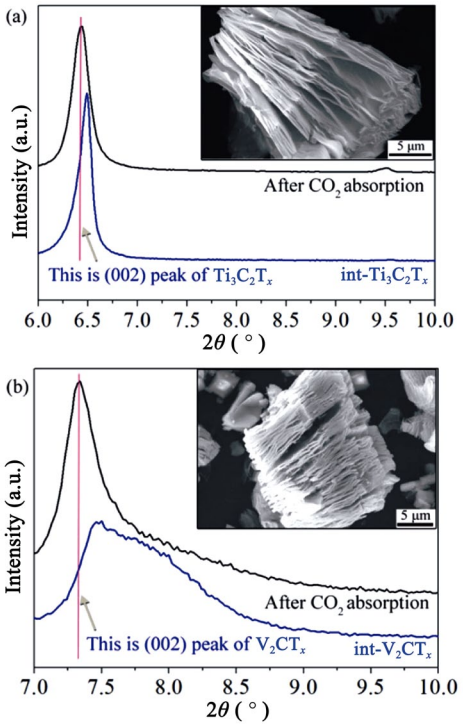

Fig. 7 XRD patterns and SEM images of (a) int-$Ti_3C_2T_x$ and (b) int-V_2CT_x after CO_2 absorption.

Theoretical calculation has similar conclusion. Based on the calculation [31], the adsorption energy of CO_2 on MXene with O termination is –0.14 eV and charge transfer is –0.007 eV. The adsorption is deemed as physical adsorption. However, this adsorption also has some chemical adsorption features, such as the unclosed hysteresis loop during desorption. Thus, the mechanism is not fully clear and more work is needed to clarify the mechanism.

Because the surface of all MXenes is terminated by F/O/OH, the adsorption properties of MXene must be affected by the type and concentration of these termination groups, which can be estimated from the results of XPS. Table 2 lists the atomic concentrations obtained from XPS. As shown in Table 2, the main surface terminations of MXenes are O and F. For $Ti_3C_2T_x$, the concentration of F is higher than that of O. For V_2CT_x, the concentration of O is higher than that of F. However, to fully understand the impact of termination, MXenes with the same chemical composition and different terminations should be made and tested,

Table 2 Atomic concentration (%) estimated from XPS of $Ti_3C_2T_x$ and V_2CT_x

Sample	Ti 2p	V 2p	C 1s	O 1s	F 1s	Na 1s	Al 2p	Cl 2p
$Ti_3C_2T_x$	13.23	—	35.59	18.24	29.19	0.18	3.04	0.53
V_2CT_x	—	9.54	41.99	35.58	6.88	0.29	4.82	0.9

which will be reported in the future.

It is noted that the adsorbed amount of $Ti_3C_2T_x$ is much larger than that of V_2CT_x. This is a little surprise to us because V_2CT_x theoretically has higher SSA than $Ti_3C_2T_x$. Normally, higher SSA results in higher adsorbed amount. Thus, V_2CT_x has been supposed to have higher capacity than $Ti_3C_2T_x$. If totally exfoliated to single cell layers, every V_2CT_x layer has two V layers and one C layer while every $Ti_3C_2T_x$ layer has three Ti layers and two C layers. The theoretical SSA of V_2CO_2 is 589 m^2/g, while that of $Ti_3C_2O_2$ is 496 m^2/g. The inconsistent relation between adsorbed amount and theoretical SSA can be explained by the exfoliation degree of the two MXenes. The exfoliation of $Ti_3C_2T_x$ is very easy. It is the first MXene reported to be prepared [7]. Thus, higher exfoliation degree is easily to be achieved. In this paper, the SSA of int-$Ti_3C_2T_x$ is 66 m^2/g, 14% of theoretical SSA. However, the exfoliation of V_2CT_x is very difficult. High pure V_2CT_x MXene was first made in 2017 [17], 6 years later than the preparation of high pure $Ti_3C_2T_x$. Thus, the exfoliation degree of V_2CT_x is usually low. In this paper, the SSA of int-V_2CT_x is 19 m^2/g, only 3.3% of theoretical SSA. Most V_2CT_x sheets should be multilayer rather than single layer. Therefore, although V_2CT_x has higher theoretical absorbed amount, in this paper, $Ti_3C_2T_x$ has higher capacity to adsorb CO_2 because $Ti_3C_2T_x$ is easily exfoliated. The achieved capacity of $Ti_3C_2T_x$ is 5.79 mmol/g. If $Ti_3C_2T_x$ MXene with theoretical SSA (100% exfoliated) can be made in the future, the theoretical capacity would be 44.2 mmol/g.

In order to evaluate the capacity of MXenes as CO_2 sorbent under high pressure, we compared MXenes with other sorbents. Zeolite 13X has the capacity of 7.38 mmol/g [44] and porous polymers have the capacity of 11.9 mmol/g [45]. The first reported capacity of $Ti_3C_2T_x$ MXene (5.79 mmol/g) is close to the capacity of those common sorbents. And MXene's capacity can be improved with better exfoliation process to make MXene with higher SSA. This can be proved by the comparison the capacities of as-$Ti_3C_2T_x$ and int-$Ti_3C_2T_x$. The theoretical capacity of $Ti_3C_2T_x$ is 44.2 mmol/g, which is already close to the capacity of MOF (54.4 mmol/g) [2]. Additionally, MXenes are not water sensitive. Water molecules can come into or come out of the interlayer space of MXenes and the pore structure of MXene will not be changed.

More importantly, the density of $Ti_3C_2O_2$ is much higher than most common CO_2 sorbents. For example, the packing density of polypyrrole-derived carbons is 0.25–0.38 g/cm^3 [46]. The apparent density of $Ti_3C_2O_2$ discs compacted under pressure of 10 MPa is 3.87 g/cm^3. If the unit of CO_2 uptake is changed from gravimetric uptake (per g) to volumetric uptake (per cm^3), which can be calculated by multiplying the adsorbed amount value in Fig. 6 by density of absorbent, the CO_2 volumetric uptake can be as high as 502 $V \cdot v^{-1}$ for int-$Ti_3C_2T_x$. And for fully exfoliated $Ti_3C_2T_x$, the theoretic volumetric uptake can be 3788 $V \cdot v^{-1}$. These values are very high, compared with 400 $V \cdot v^{-1}$ for polypyrrole-derived carbons with SSA of 3934 m^2/g and 130 $V \cdot v^{-1}$ for MOF-210 with SSA of 6240 m^2/g [46]. Thus MXenes are very promising CO_2 sorbent with excellent volumetric uptake capacity. The high volumetric capacity means CO_2 can be stored in a tank with very small volume. This is important for the applications that require small dimensions, such as adsorption of gas from landfills, etc.

4 Conclusions

MXene powders ($Ti_3C_2T_x$ and V_2CT_x) were prepared by exfoliating MAX phases (Ti_3AlC_2 and V_2AlC, respectively) powders in the solution of NaF and hydrochloric acid (HCl). XRD and Raman data show that MXenes were obtained successfully. As-prepared MXenes can be further exfoliated to increase SSA by intercalation with DMSO. Although V_2CT_x has higher theoretical SSA than $Ti_3C_2T_x$, $Ti_3C_2T_x$ made in this paper has better structure and higher SSA than V_2CT_x because $Ti_3C_2T_x$ is easily exfoliated.

The CO_2 adsorption properties of $Ti_3C_2T_x$ MXene and V_2CT_x MXene were tested in this paper. It was found that MXenes are promising sorbent for CO_2 capture. Intercalated MXenes have obviously higher adsorbed amount than as-prepared MXenes. Int-$Ti_3C_2T_x$ with the SSA of 66 m^2/g has the capacity of 5.79 mmol/g, which is close to the capacity of many common sorbents. The theoretical capacity of $Ti_3C_2T_x$ with the SSA of 496 m^2/g is 44.2 mmol/g, which is close to the capacity of MOF. Additionally, due to high pack density, MXenes have very high volume-uptake capacity. The capacity of int-$Ti_3C_2T_x$ measured in this paper is 502 $V \cdot v^{-1}$. This value is already higher than volume capacity of most known sorbents.

Acknowledgements

This work was supported by National Natural Science

Foundation of China (Grant Nos. 51472075 and 51772077), Program for Innovative Research Team (in Science and Technology) in the University of Henan Province (Grant No. 19IRTSTHN027), Natural Science Foundation of Henan Province (Grant Nos. 182300410228 and 182300410275).

References

[1] Balasubramanian R, Chowdhury S. Recent advances and progress in the development of graphene-based adsorbents for CO_2 capture. *J Mater Chem A* 2015, **3**: 21968–21989.

[2] Furukawa H, Ko N, Go YB, *et al.* Ultrahigh porosity in metal-organic frameworks. *Science* 2010, **329**: 424–428.

[3] Yu J, Le Y, Cheng B. Fabrication and CO_2 adsorption performance of bimodal porous silica hollow spheres with amine-modified surfaces. *RSC Adv* 2012, **2**: 6784–6791.

[4] Huang K, Chai S-H, Mayes RT, *et al.* Significantly increasing porosity of mesoporous carbon by $NaNH_2$ activation for enhanced CO_2 adsorption. *Microporous Mesoporous Mater* 2016, **230**: 100–108.

[5] Huong P-T, Lee B-K. Improvement of selective separation of CO_2 over N_2 by transition metal–exchanged nano-zeolite. *Microporous Mesoporous Mater* 2017, **241**: 155–164.

[6] Saleh M, Baek SB, Han ML, *et al.* Triazine-based microporous polymers for selective adsorption of CO_2. *J Phys Chem C* 2015, **119**: 5395–5402

[7] Naguib M, Kurtoglu M, Presser V, *et al.* Two-dimensional nanocrystals produced by exfoliation of Ti_3AlC_2. *Adv Mater* 2011, **23**: 4248–4253.

[8] Hu Q, Wang H, Wu Q, *et al.* Two-dimensional Sc_2C: A reversible and high-capacity hydrogen storage material predicted by first-principles calculations. *Int J Hydrogen Energ* 2014, **39**: 10606–10612.

[9] Naguib M, Mochalin VN, Barsoum MW, *et al.* Two-dimensional materials: 25th Anniversary Article: MXenes: A new family of two-dimensional materials. *Adv Mater* 2014, **26**: 982–982.

[10] Ling C, Shi L, Ouyang Y, *et al.* Transition metal-promoted V_2CO_2 (MXenes): A new and highly active catalyst for hydrogen evolution reaction. *Adv Sci* 2016, **3**: 1600180.

[11] Guo Z, Zhou J, Zhu L, *et al.* MXene: A promising photocatalyst for water splitting. *J Mater Chem A* 2016, **4**: 11446–11452.

[12] Ran J, Gao G, Li F-T, *et al.* Ti_3C_2 MXene co-catalyst on metal sulfide photo-absorbers for enhanced visible-light photocatalytic hydrogen production. *Nat Commun* 2017, **8**: 13907.

[13] Feng A, Yu Y, Jiang F, *et al.* Fabrication and thermal stability of NH_4HF_2-etched Ti_3C_2 MXene. *Ceram Int* 2017, **43**: 6322–6328.

[14] Berdiyorov GR, Mahmoud KA. Effect of surface termination on ion intercalation selectivity of bilayer $Ti_3C_2T_2$ (T = F, O and OH) MXene. *Appl Surf Sci* 2017, **416**: 725–730.

[15] Zhao M-Q, Ren CE, Ling Z, *et al.* Flexible MXene/carbon nanotube composite paper with high volumetric capacitance. *Adv Mater* 2015, **27**: 339–345.

[16] Liu F, Zhou A, Chen J, *et al.* Preparation and methane adsorption of two-dimensional carbide Ti_2C. *Adsorption* 2016, **22**: 915–922.

[17] Liu F, Zhou J, Wang S, *et al*. Preparation of high-purity V_2C MXene and electrochemical properties as Li-ion batteries. *J Electrochem Soc* 2017, **164**: A709–A713.

[18] Urbankowski P, Anasori B, Makaryan T, *et al.* Synthesis of two-dimensional titanium nitride Ti_4N_3 (MXene). *Nanoscale* 2016, **8**: 11385–11391.

[19] Zhou J, Zha X, Zhou X, *et al.* Synthesis and electrochemical properties of two-dimensional hafnium carbide. *ACS Nano* 2017, **11**: 3841–3850.

[20] Ghidiu M, Naguib M, Shi C, *et al.* Synthesis and characterization of two-dimensional Nb_4C_3 (MXene). *Chem Commun* 2014, **50**: 9517–9520.

[21] Mashtalir O, Naguib M, Mochalin VN, *et al.* Intercalation and delamination of layered carbides and carbonitrides. *Nat Commun* 2013, **4**: 1716–1722.

[22] Meshkian R, Näslund L-Å, Halim J, *et al.* Synthesis of two-dimensional molybdenum carbide, Mo_2C, from the gallium based atomic laminate Mo_2Ga_2C. *Scripta Mater* 2015, **108**: 147–150.

[23] Han M, Yin X, Li X, *et al.* Laminated and two-dimensional carbon-supported microwave absorbers derived from MXenes. *ACS Appl Mater Interface* 2017, **9**: 20038–20045

[24] Li X, Yin X, Han M, *et al.* A controllable heterogeneous structure and electromagnetic wave absorption properties of Ti_2CT_x MXene. *J Mater Chem C* 2017, **5**: 7621–7628.

[25] Liu J, Zhang H-B, Sun R, *et al.* Hydrophobic, flexible, and lightweight MXene foams for high-performance electromagnetic-interference shielding. *Adv Mater* 2017, **29**: 1702367.

[26] Lukatskaya MR, Mashtalir O, Ren CE, *et al.* Cation intercalation and high volumetric capacitance of two-dimensional titanium carbide. *Science* 2013, **341**: 1502– 1505.

[27] Gao Y, Wang L, Li Z, *et al.* Electrochemical performance of Ti_3C_2 supercapacitors in KOH electrolyte. *J Adv Ceram* 2015, **4**: 130–134.

[28] Berdiyorov GR. Effect of lithium and sodium ion adsorption on the electronic transport properties of Ti_3C_2 MXene. *Appl Surf Sci* 2015, **359**: 153–157.

[29] Naguib M, Come J, Dyatkin B, *et al.* MXene: A promising transition metal carbide anode for lithium-ion batteries. *Electrochem Commun* 2012, **16**: 61–64.

[30] Xie Y, Dall'Agnese Y, Naguib M, *et al.* Prediction and characterization of MXene nanosheet anodes for non-lithium-ion batteries. *ACS Nano* 2014, **8**: 9606–9615.

[31] Yu X, Li Y, Cheng JB, *et al.* Monolayer Ti_2CO_2: A promising candidate for NH_3 sensor or capturer with high sensitivity and selectivity. *ACS Appl Mater Interfaces* 2015, **7**: 13707–13713.

[32] Hu Q, Sun D, Wu Q, *et al.* MXene: A new family of promising hydrogen storage medium. *J Phys Chem A* 2013, **117**: 14253–14260.

[33] Liu F, Zhou A, Chen J, *et al.* Preparation of Ti_3C_2 and Ti_2C MXenes by fluoride salts etching and methane adsorptive properties. *Appl Surf Sci* 2017, **416**: 781–789.

[34] Li L, Zhou A, Xu L, *et al.* Synthesis of high pure Ti_3AlC_2 and Ti_2AlC powders from TiH_2 powders as Ti source by tube furnace. *J Wuhan Univ Technol Mater Sci Ed* 2013, **28**: 882–887.

[35] Zhou A, Sun D, Zhang H, *et al.* Synthesis of V_2AlC powders and their corrosion behavior in hydrofluoric acid. *Rare Metal Mater Eng* 2015, **44**: 507–510. (in Chinese)

[36] Wang B, Zhou A, Hu Q, *et al.* Synthesis and oxidation resistance of V_2AlC powders by molten salt method. *Int J Appl Ceram Tec* 2017, **14**: 873–879.

[37] Li Z, Wang L, Sun D, *et al.* Synthesis and thermal stability of two-dimensional carbide MXene Ti_3C_2. *Mat Sci Eng B* 2015, **191**: 33–40.

[38] Ghidiu M, Halim J, Kota S, *et al.* Ion-exchange and cation solvation reactions in Ti_3C_2 MXene. *Chem Mater* 2016, **28**: 3507–3514.

[39] Naguib M, Halim J, Lu J, *et al.* New two-dimensional niobium and vanadium carbides as promising materials for Li-ion batteries. *J Am Chem Soc* 2013, **135**: 15966–15969.

[40] Wang L, Zhang H, Wang B, *et al.* Synthesis and electrochemical performance of $Ti_3C_2T_x$ with hydrothermal process. *Electron Mater Lett* 2016, **12**: 702–710.

[41] Presser V, Naguib M, Chaput L, *et al.* First-order Raman scattering of the MAX phases: Ti_2AlN, $Ti_2AlC_{0.5}N_{0.5}$, Ti_2AlC, $(Ti_{0.5}V_{0.5})_2AlC$, V_2AlC, Ti_3AlC_2, and Ti_3GeC_2. *J Raman Spectrosc* 2012, **43**: 168–172.

[42] Champagne A, Shi L, Ouisse T, *et al.* Electronic and vibrational properties of V_2C-based MXenes: From experiments to first-principles modeling. *Phys Rev B* 2018, **97**: 115439.

[43] Wickramaratne NP, Jaroniec M. Activated carbon spheres for CO_2 adsorption. *ACS Appl Mater Interfaces* 2013, **5**: 1849–1855.

[44] Cavenati S, Grande CA, Rodrigues AE. Adsorption equilibrium of methane, carbon dioxide, and nitrogen on zeolite 13X at high pressures. *J Chem Eng Data* 2004, **49**: 1095–1101.

[45] Bracco S, Piga D, Bassanetti I, *et al.* Porous 3D polymers for high pressure methane storage and carbon dioxide capture. *J Mater Chem A* 2017, **5**: 10328–10337.

[46] Cox M, Mokaya R. Ultra-high surface area mesoporous carbons for colossal pre combustion CO_2 capture and storage as materials for hydrogen purification. *Sustainable Energy Fuels* 2017, **1**: 1414–1424.